

This is an Accepted Manuscript version of the following article, accepted for publication in:

A. Alacano, J. J. Valera, G. Abad and P. Izurza, "Power-Electronic-Based DC Distribution Systems for Electrically Propelled Vessels: A Multivariable Modeling Approach for Design and Analysis," in IEEE Journal of Emerging and Selected Topics in Power Electronics, vol. 5, no. 4, pp. 1604-1620, Dec. 2017.

DOI: <https://doi.org/10.1109/JESTPE.2017.2730855>

© 2017 IEEE. Personal use of this material is permitted. Permission from IEEE must be obtained for all other uses, in any current or future media, including reprinting/republishing this material for advertising or promotional purposes, creating new collective works, for resale or redistribution to servers or lists, or reuse of any copyrighted component of this work in other works.

Power Electronics Based DC Distribution Systems for Electrically Propelled Vessels: A Multivariable Modeling Approach for Design and Analysis

Argiñe Alacano, Juan José Valera, Gonzalo Abad, and Pedro Izurza

Presented in 17th IEEE Workshop on Control and Modeling for Power Electronics (COMPEL), Trondheim, Norway, 27 – 30 June, 2016.

Abstract—The benefits of using Power Electronics Based DC Distribution Systems in electrically propelled vessels are well known. However, some aspects must be deeply analyzed to guarantee a safe, robust and stable system by design. This paper presents a multivariable DC Distribution System mathematical model, where all the transmission lines and filters impedances are considered. The model has been tackled under a holistic approach in which the average small-signal model of the drives/converters can be easily added and ‘connected’ to the main grid model. The stability and power quality analysis, as well as the design and tuning of controls and active damping strategies can be conducted through this mathematical model at low computational cost. The usefulness of this model in the early design stages is thus presented in this paper through its application over a realistic design scenario and the performance of the proposed model is proven into a real test bench which presents a configuration and architecture quite close to the one used in a real vessel. The carried out tests prove the suitability of the proposed model, becoming a significant tool to get an improved design.

Index Terms—DC power distribution system; multivariable modeling; design approach; power system dynamics, power system stability.

A. Alacano and G. Abad are with the Electronics and Computing Department, Mondragon University, 20500 Mondragon, Spain (e-mail: aalacano@mondragon.edu, gabad@mondragon.edu).

J.J. Valera and P. Izurza are with the Industry and Marine Drives Department, Ingeteam Power Technology S.A., 48170 Zamudio, Spain (email: juanjose.valera@ingetteam.com, pedro.izurza@ingetteam.com).

I. INTRODUCTION

The benefits of using power electronic based DC distribution systems (PEB-DCDS) for electrically propelled vessels are well analyzed and documented, especially under the assumption of operations with high variability load profiles [1], [2]. Among others, the energy efficiency, the fuel consumption and, therefore, the emissions can be highly improved mainly due to the operation of the gensets at variable speed; the energy storage systems can be integrated easier; and the electrical power plant size and weight can be optimized. According to the different PEB-DCDS architectures or topologies, the one that offers more benefits in terms of energy efficiency, cost and size is the distributed topology [2]. In such topology, a very long DC bus is placed throughout the vessel passing very close to the main load converters thus minimizing the AC power wiring (just in the case of AC loads). Regardless the topology, i.e. centralized, distributed or mixed, the PEB-DCDS is usually divided in two or even more zones for safety reasons as in the case of offshore vessels and navy applications respectively.

The gensets (power sources) can be connected to the DC bus through AC-DC diode (DR), thyristor (TR) or active front end rectifiers (AFE). The energy storage systems (that can be considered as power sources or DC loads) and other DC loads can be connected directly or through DC-DC converters to the DC bus depending on their voltage levels and the defined control or energy management strategy. Regarding the AC loads, they are connected to the DC bus through DC-AC inverters. Especially for low voltage applications, the three-phase voltage source converter (VSC) topology is commonly used for both the AFE (AC-DC) and the inverters (DC-AC), so from now on in the text, the term VSC will be used for referring the converters on the PEB-DCDS. A diagram of a distributed PEB-DCDS with two zones is shown in Fig. 1., where the common voltage levels are 1100V for the DC bus and 690V for the AC electric motors & generators in vessels with a total installed power typically from 5 to 30MW.

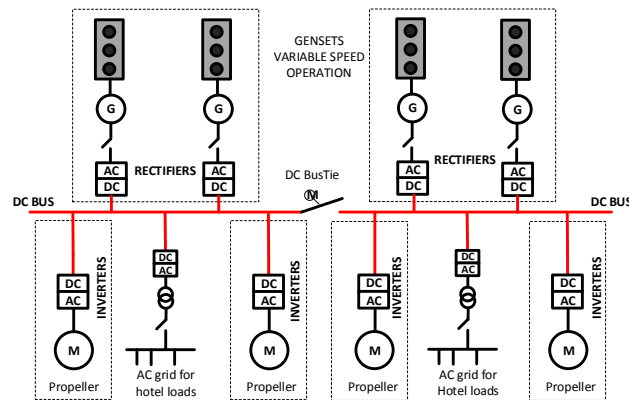


Fig. 1. A DC grid with distributed topology for an offshore supply vessel.

Beyond the energy efficiency and the safety issues, the stability, the dynamic control behavior and the power quality requirements must be also considered from the early stages when designing a PEB-DCDS. A dynamic model capturing the transient and the steady state responses is mandatory for analyzing these requirements thus supporting the design decision making. The use of an accurate and faithful dynamic model is the key to get a robust and optimal design.

In the design problem, the inputs are: (a) the characteristics of the VSCs connected to the grid such as the capacitance of the capacitors at the DC side of the VSCs, the nominal power, the required dynamic control bandwidth, the switching frequency and the characteristics of the VSCs modulation technique in order to estimate the current harmonics at the DC link; (b) the vessel operation modes including an estimation of the main loads power profiles to evaluate, at least, the local stability and the power quality for the most representative vessel operating points; and (c) the layout of the electrical and machinery rooms in the vessel.

The design variables (outputs of the problem) are: (a) the routing of the PEB-DCDS transmission lines and the material used (power cables or bus-duct); (b) the passive filters or smoothing impedances placed at the DC side of the converters if needed; (c) the active damping control strategies (virtual impedances) if needed including their tuning.

The objectives to be ensured and optimized are: (a) the PEB-DCDS must be stable for all the operation modes and operating points of the vessel offering well-enough stability margins (well damped system) [3]–[11], (b) the power quality of the PEB-DCDS (current and voltage ripples) must fulfill the requirements established by the designers and by the Class Societies; (c) the dynamic response of the voltage control in the PEB-DCDS must fulfill the requirements specified by the designers and by the Class Societies in order to ensure a proper and safe operation of the vessel power system; (d) Obviously the cost of the solution must be reasonable and competitive.

Tightly regulated load converters usually behave as constant power loads (CPLs) from the source side point of view, exhibiting negative incremental impedance which jeopardizes the stability of the PEB-DCDS [3]. Moreover and especially in the distributed topology, the interaction of the impedances on the PEB-DCDS transmission lines and the LC filters – sometimes placed on the DC side/link of the VSCs - can cause some system resonances. Depending on the frequency, magnitude and phase of these resonance points, the whole system stability may deteriorate (low damped or even unstable PEB-DCDS). Additionally, the power quality on the PEB-DCDS (voltage and current ripples) can be affected too, especially when the main harmonics injected by the VSC at the DC link (due to its switching operation and vector modulation technique) just energize the system resonances of high magnitude. The PEB-DCDS behaves as a complex multivariable and strongly coupled system, where the systemic and holistic approach is mandatory to ensure a safe and robust design.

This paper proposes and describes a model driven methodology to design and analyze a PEB-DCDS for electrically propelled vessels that is focused on the stability, the dynamic control behavior and the power quality. A detailed description of the proposed PEB-DCDS multivariable model is presented in the first part of the paper. The usefulness of this model is presented in the second part of the paper through its application over a realistic design scenario. Finally, an experimental validation of the multivariable modeling approach is provided by using a test bench which presents a configuration and architecture that is quite close to the one used in a real vessel.

Thus, the work presented in this paper can be contextualized within the generic framework of research so called DC microgrids [12]. Uncountable efforts are being made by the research community in this direction. Considering the many architectures and power circuits proposed [13], the multivariable modeling approach proposed in this paper, emphasizes its analysis on AC-DC and DC-AC VSC topologies, since in nowadays vessels, these type of converters are the most employed ones (most of the generation and load are in AC). However, note that the modeling approach proposed can be easily extended to consider also DC-DC converters or even diode based AC-DC converters.

It has to be remarked that much research has been also made in developing autonomous operation of converters connected to the DC microgrid, by means of current or power sharing control methods [14]–[17]. The autonomous operation of AFE rectifiers is not considered in this work, which in fact, is a common solution in nowadays vessels with PEB-DCDS. Thus, only one DC bus voltage controller is supposed in this work [18] and the power required to regulate the DC bus voltage is divided among the existing intercommunicated AFE rectifiers, according to the master-slave and load sharing criteria. However, once again the proposed modeling approach can also integrate different control methods and strategies for autonomous operation.

Finally, it has to be mentioned that many other necessary works and challenging topics related to PEB-DCDS for vessels can be found in specialized literature, such as for instance: solid state circuit breaker protections [19], innovative hybrid energy storage systems [20] or analysis for -Size and weight computation [21]. However, they are out of the scope of the analysis of this paper.

II. PEB-DCDS AVERAGE SMALL-SIGNAL MODEL

This section presents a multivariable and modular model of a PEB-DCDS. The model is very useful on the early design stages, as it allows understanding the system behavior in terms of stability and power quality at low computational cost. In this approach, the different subsystems that compose the PEB-DCDS are modeled separately for its particular comprehension. Then, all the subsystems models are mathematically ‘inter connected’ to get the mathematical model of the whole system (holistic approach). An example of a PEB-DCDS with 4x branches is shown in Fig. 2, where a VSC operating as an AFE rectifier (DC bus voltage control) is placed at the first branch and 2x VSCs working as CPL are placed at the branches 2 and 3. A sub (inner) PEB-DCDS of 3x branches – with a CPL-VSC in each branch - is placed at the (outer) branch 4.

In Fig. 2, $(z_i, z_s, z_{si}, z_{bi}, z_{bsi})$ are the cables, bus-bars or transmission lines impedances, (C_i, C_{si}) are the capacitors at the DC link of the VSCs, and $(z_{fi}, z_{fs}, z_{fsi})$ are, if needed, the smoothing or filter impedances. Note that the sub-index i is referring to the branch and VSC number, whereas the sub-index ‘ s ’ is referring to the branches of the inner grid. The outer and inner PEB-DCDS models are separately modelled from their respective equivalent electrical circuits and later mathematically ‘inter-connected’. This fact helps the adaptability of the modeling approach to different possible configurations.

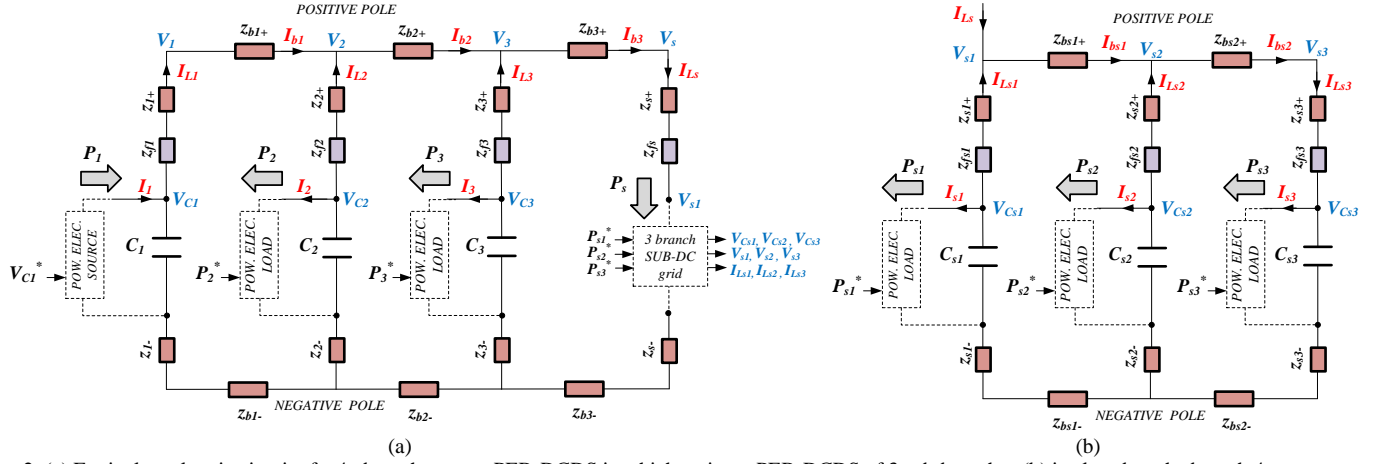


Fig. 2. (a) Equivalent electric circuit of a 4x branches outer PEB-DCDS in which an inner PEB-DCDS of 3 sub-branches (b) is placed on the branch 4.

The outer and inner PEB-DCDS models are separately modelled from their respective equivalent electrical circuits and later mathematically ‘inter-connected’.

A. Transmission lines impedances model

In marine applications, the main distribution power wiring is generally built by using cables or bus-bars into a bus-duct assembly. In this work, the impedances of the lines are modeled as $R + j\omega L$ impedances for both cases, where the R and L magnitudes can be estimated by using the resistivity formula and the method proposed in [22], [23] respectively. These methods deduce an equivalent circuit which consist of a resistance, a self-inductance and a mutual inductance, as depicted in Fig. 3, based on the dimensions and geometry of the cables or bus-ducts and the distance among them, as well as on the material used. Some equivalent R and L values are presented in section III, which represent the behavior of cables and bus-ducts in a sufficiently accurate manner at least, up to frequencies of 2kHz, or even more, [24].

In general, by using bus bars instead of cables involves reducing the line impedances on the circuit and, therefore, reducing the bus own losses as well as the risk of poor stability or even instability problems especially when using long DC buses and powers in the range of several megawatts. Nevertheless, the lay out of the bus-duct (bus bar) and its assembly especially in long and high distributed topologies is more complex and challenging.

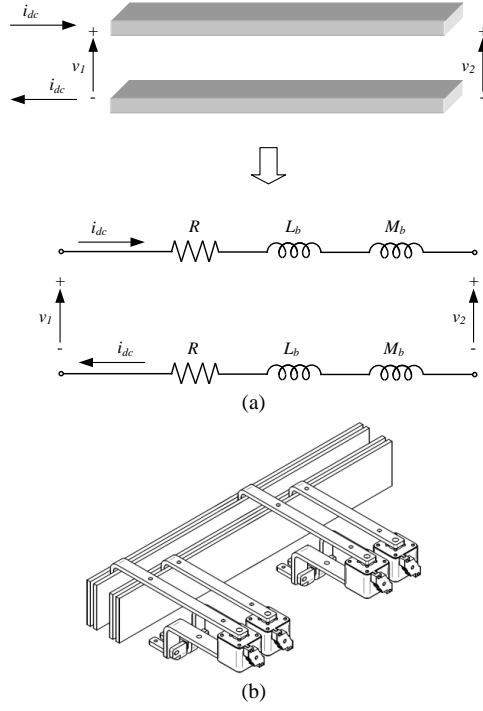


Fig. 3. (a) Parallelism between simple bus-bars geometry and equivalent R - L impedance. (b) Illustrative example of bus-bar geometries for (PEB-DCDS).

B. Outer Grid Model

According to Fig. 2a, the voltages (V_i , V_{Ci}) together with the currents I_{Li} are the outputs of the outer grid model, where $i=1, 2, 3, s$. The VSC DC-link currents I_j together with the voltage V_{Sj} are the inputs, where $j=1, 2, 3$. Under the assumption of time-invariant parameters, a multivariable linear model can be constructed (1), where the matrixes $Z(s)$, $Z_p(s)$ and $G(s)$ are composed by transfer function elements in the Laplace domain (2)-(9). For simplicity reasons, the impedances have been grouped in the model: $z_i = z_{i+} + z_{i-} + z_{fi}$, $z_s = z_{s+} + z_{s-} + z_{fs}$ and $z_{bi} = z_{bi+} + z_{bi-}$.

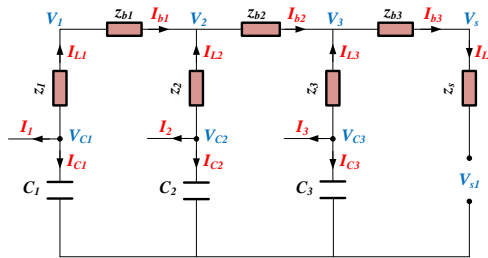


Fig. 4. Simplified electric equivalent circuit of the outer grid of the PEB-DCDS.

$$\begin{bmatrix} V_{Cm} \\ V_m \\ I_{Lm} \end{bmatrix} = [Z_{bus_ext}] \cdot \begin{bmatrix} I_m \\ V_{S1} \end{bmatrix} \quad m = 1, 2, 3 \quad (1)$$

$$[Z_{bus_ext}] = \begin{bmatrix} [Z] \\ [Z_p] \\ [G][Z_p] \end{bmatrix} \quad (2)$$

$$[Z] = ([J][G] + [J_1])[Z_p] \quad (3)$$

$$[J] = \begin{bmatrix} z_1 & 0 & 0 & 0 \\ 0 & z_2 & 0 & 0 \\ 0 & 0 & z_3 & 0 \end{bmatrix} \quad (4)$$

$$[J_1] = \begin{bmatrix} 1 & 0 & 0 & 0 \\ 0 & 1 & 0 & 0 \\ 0 & 0 & 1 & 0 \end{bmatrix} \quad (5)$$

$$[G] = \begin{bmatrix} \frac{1}{z_{b1}} & \frac{-1}{z_{b1}} & 0 & 0 \\ \frac{-1}{z_{b1}} & \frac{1}{z_{b1}} + \frac{1}{z_{b2}} & \frac{-1}{z_{b2}} & 0 \\ 0 & \frac{-1}{z_{b2}} & \frac{1}{z_{b2}} + \frac{1}{z_{b3}} & \frac{-1}{z_{b3}} \\ 0 & 0 & \frac{-1}{z_{b3}} & \frac{1}{z_{b3}} \end{bmatrix} \quad (6)$$

$$[Z_p] = (1 - [F][G])^{-1}[H] \quad (7)$$

$$[F] = \begin{bmatrix} \frac{-z_1 C_1 s - 1}{C_1 s} & 0 & 0 & 0 \\ 0 & \frac{-z_2 C_2 s - 1}{C_2 s} & 0 & 0 \\ 0 & 0 & \frac{-z_3 C_3 s - 1}{C_3 s} & 0 \\ 0 & 0 & 0 & z_s \end{bmatrix} \quad (8)$$

$$[H] = \begin{bmatrix} \frac{-1}{C_1 s} & 0 & 0 & 0 \\ 0 & \frac{-1}{C_2 s} & 0 & 0 \\ 0 & 0 & \frac{-1}{C_3 s} & 0 \\ 0 & 0 & 0 & 1 \end{bmatrix} \quad (9)$$

C. Inner Grid Model

From Fig. 2b and applying the same procedure as in the outer grid model, the inner grid model (10) can be obtained from (11)-(18). For simplicity reasons, the impedances have been grouped in the model: $z_{si} = z_{si+} + z_{si-} + z_{fsi}$ and $z_{bsi} = z_{bsi+} + z_{bsi-}$.

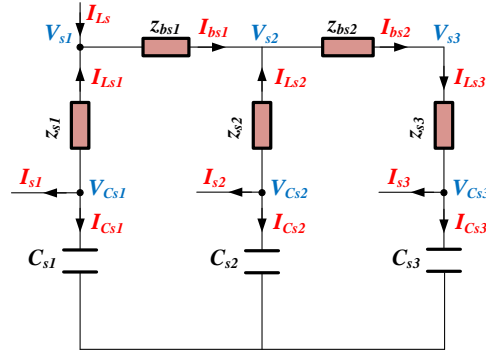


Fig. 5. Simplified electric equivalent circuit of the inner grid of the PEB-DCDS.

$$\begin{bmatrix} V_{sn} \\ V_{Csn} \\ I_{Lsn} \end{bmatrix} = [Z_{bus_int}] \begin{bmatrix} I_{Ls} \\ I_{sn} \end{bmatrix} \quad n = 1,2,3 \quad (10)$$

$$[Z_{bus_int}] = \begin{bmatrix} [Z'] \\ [Z_p'] \\ [G'] [Z_p'] + [G_2'] \end{bmatrix} \quad (11)$$

$$[Z] = [J'] ([G'] [Z_p'] + [G_2']) + [Z_p'] \quad (12)$$

$$[J'] = \begin{bmatrix} z_{s1} & 0 & 0 \\ 0 & z_{s2} & 0 \\ 0 & 0 & -z_{s3} \end{bmatrix} \quad (13)$$

$$[G'] = \begin{bmatrix} \frac{1}{z_{bs1}} & \frac{-1}{z_{bs1}} & 0 \\ \frac{-1}{z_{bs1}} & \frac{1}{z_{bs1}} + \frac{1}{z_{bs2}} & \frac{-1}{z_{bs2}} \\ 0 & \frac{1}{z_{bs2}} & \frac{-1}{z_{bs2}} \end{bmatrix} \quad (14)$$

$$[G_2'] = \begin{bmatrix} 0 & 0 & 0 & -1 \\ 0 & 0 & 0 & 0 \\ 0 & 0 & 0 & 0 \end{bmatrix} \quad (15)$$

$$[Z_p'] = (1 - [F'] [G'])^{-1} ([F'] [G_2'] + [H']) \quad (16)$$

$$[F'] = \begin{bmatrix} \frac{-z_{s1} C_{s1} s - 1}{C_{s1} s} & 0 & 0 \\ 0 & \frac{-z_{s2} C_{s2} s - 1}{C_{s2} s} & 0 \\ 0 & 0 & \frac{z_{s3} C_{s3} s + 1}{C_{s3} s} \end{bmatrix} \quad (17)$$

$$[H'] = \begin{bmatrix} \frac{-1}{C_{s1}s} & 0 & 0 & 0 \\ 0 & \frac{-1}{C_{s2}s} & 0 & 0 \\ 0 & 0 & \frac{-1}{C_{s3}s} & 0 \end{bmatrix} \quad (18)$$

Therefore, as a matter of example, next equations show how the inner grid I_{Ls1} , I_{Ls2} , I_{Ls3} currents result, in function of the input currents I_{Ls} , I_{s1} , I_{s2} , I_{s3} , after combining and arranging all the corresponding matrixes ($C_s = C_{s1} = C_{s2} = C_{s3}$ has been considered):

$$\begin{bmatrix} I_{Ls1} \\ I_{Ls2} \\ I_{Ls3} \end{bmatrix} = \begin{bmatrix} \frac{-C_s^2(Z_{eq2})s^2 - C_s(Z_{eq1})s - 1}{den(s)} & \frac{-C_s(z_{s3} - z_{s2} - z_{sb2})s - 2}{den(s)} & \frac{C_s(z_{s3} + z_{sb2})s + 1}{den(s)} & \frac{C_s(z_{s2})s + 1}{den(s)} \\ \frac{-C_s^2(z_{s1}z_{s3} + z_{s1}z_{sb2})s^2 - C_s(z_{s1} + z_{s3} + z_{sb2})s - 1}{den(s)} & \frac{C_s(z_{s3} + z_{sb2})s + 1}{den(s)} & \frac{-C_s(z_{s1} + z_{s3} + z_{sb1} + z_{sb2})s - 2}{den(s)} & \frac{C_s(z_{s1} + z_{sb1})s + 1}{den(s)} \\ \frac{-C_s^2(z_{s1}z_{s2})s^2 - C_s(z_{s1} + z_{s2})s + 1}{den(s)} & \frac{-C_s(z_{s2})s - 1}{den(s)} & \frac{-C_s(z_{s1} + z_{sb1})s - 1}{den(s)} & \frac{C_s(z_{s2} + z_{sb1})s + 2}{den(s)} \end{bmatrix} \begin{bmatrix} I_{Ls} \\ I_{s1} \\ I_{s2} \\ I_{s3} \end{bmatrix} \quad (19)$$

Being:

$$den(s) = C_s^2(z_{s1}(z_{s2} + z_{s3} + z_{sb2}) + z_{s2}(z_{s3} + z_{sb1} + z_{sb2}) + z_{sb1}(z_{s3} + z_{sb2}))s^2 + C_s(z_{s1} + z_{s2} + z_{s3} + z_{sb1} + z_{sb2})s + 3 \quad (20)$$

And:

$$Z_{eq1} = z_{s2} + z_{s3} + z_{sb1} + z_{sb2} \quad (21)$$

$$Z_{eq2} = z_{s2}(z_{s3} + z_{sb1} + z_{sb2}) + z_{sb1}(z_{s3} + z_{sb2}) \quad (22)$$

Note that all the terms that compose the currents I_{Ls1} , I_{Ls2} , I_{Ls3} , share the same denominator, which is at this stage a second order system. However, if an inductance term is considered in all the parasitic impedances of the grid (z_{s1} , z_{s2} , etc.), it will become a fourth order system with a pair of complex conjugate poles as later will be seen. Equivalent expressions can be derived for the rest of the variables of the inner grid (V_{sn} and V_{Csn}) and also, the same procedure can be applied to inner grids with different number of branches or even to the outer grid. By simple observation of the matrixes (1)-(9) and (10)-(18), the addition of new branches into the outer and inner grid models can be carefully but easily performed.

D. VSC Admittance Model

The VSCs connected to the PEB-DCDS (operating as sources or loads) are usually controlled in grid oriented vector control mode [25], [26]. The VSC models are non-linear but if linearized they depend on the VSC control loops dynamics as well as on the vessel operating/equilibrium point used for the linearization. The well-known linearized & small-signal modeling technique described in [27] and [26] is used in this paper to get the admittances models $[I_i(s)/V_{Ci}(s)]$. Two different VSC admittance models are considered in this work: the AFE rectifier controlling the DC bus voltage (AFE-VSC) and the inverter based drives operating as constant power loads (CPL-VSC). The control diagram for the case of an AFE-VSC is depicted in Fig. 6. The CPL-VSC control

diagram is similar than the one for the AFE-VSC, but a power reference is only used instead of the DC bus voltage control loop in the case of the CPL-VSC.

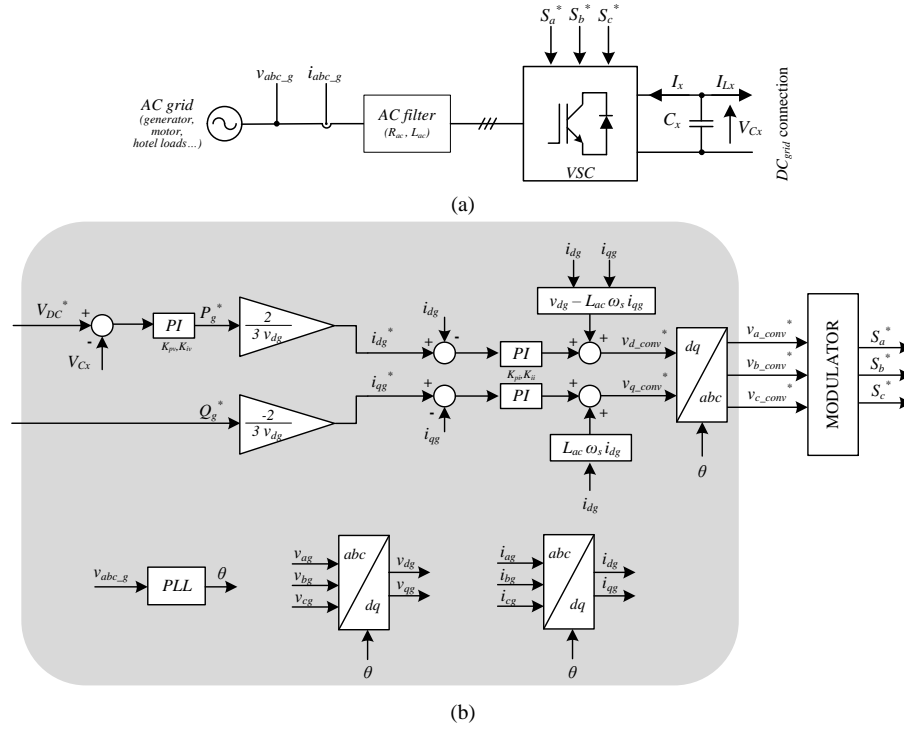


Fig. 6. AFE-VSC model. (a) Power diagram. (b) Control diagram.

Under the assumption of time-invariant parameters, a small-signal linear model can be constructed for the AFE-VSCs (23) and for the CPL-VSCs (26), where the matrixes $G_{Vref_AFE}(s)$, $G_{Vc_AFE}(s)$, $G_{Pref}(s)$ and $G_{Vc_CPL}(s)$ are composed by transfer function elements in the Laplace domain, (24)-(25) for the AFE-VSCs, and (27)-(28) for the CPL-VSCs. Note that the models depend on the equilibrium point used for the linearization: $(V_{DCo_AFE}, I_{DCo_AFE})$ in the case of the AFE-VSCs and $(V_{DCo_CPLi}, I_{DCo_CPLi})$ in the case of the CPL-VSCs. The power balance in this equilibrium point must be zero. In the case of an AFE-VSC, the DC-link voltage set point V_{DC}^* , that for the considered configuration is V_{CI}^* , together with the AFE-VSC DC-link voltage, V_{C_AFE} , form the inputs of the admittance model, while the linearized & small-signal current at the DC-link, I_{AFE} , is the output (23). In the case of a CPL-VSC, the load active power set-point, P_i^* and the DC-link voltage, V_{C_CPLi} , are the inputs while the linearized & small-signal current at the DC-link, I_{CPLi} , is the output (26).

$$\tilde{I}_{AFE} = \begin{bmatrix} G_{Vref_AFE}(s) & G_{Vc_AFE}(s) \end{bmatrix} \begin{bmatrix} \tilde{V}_{DC}^* \\ \tilde{V}_{C_AFE} \end{bmatrix} \quad (23)$$

$$G_{Vref_AFE}(s) = \left(K_{pv} + \frac{K_{iv}}{s} \right) \left(\frac{K_{pi}s + K_{ii}}{L_{ac}s^2 + (R_{ac} + K_{pi})s + K_{ii}} \right) \frac{1}{V_{DCo_AFE}} \quad (24)$$

$$G_{Vc_AFE}(s) = -G_{Vref_AFE}(s) - \frac{I_{DCo_AFE}}{V_{DCo_AFE}} \quad (25)$$

$$\tilde{I}_{CPLi} = \begin{bmatrix} G_{Pref}(s) & G_{Vc_CPL}(s) \end{bmatrix} \begin{bmatrix} \tilde{P}_i^* \\ \tilde{V}_{C_CPLi} \end{bmatrix} \quad (26)$$

$$G_{Pref}(s) = \left(\frac{K_{pi}s + K_{ii}}{L_{ac}s^2 + (R_{ac} + K_{pi})s + K_{ii}} \right) \frac{1}{V_{DCo_CPLi}} \quad (27)$$

$$G_{Vc_CPL}(s) = -\frac{I_{DCo_CPLi}}{V_{DCo_CPLi}} \quad (28)$$

Being the current loops dynamics tuned as two real equal poles (ω_{ni}) [25]:

$$\frac{K_{pi}s + K_{ii}}{L_{ac}s^2 + (R_{ac} + K_{pi})s + K_{ii}} = \frac{K_{pi}s + K_{ii}}{(s + \omega_{ni})^2} \quad (29)$$

and:

$$2\omega_{ni} = \frac{R_{ac} + K_{pi}}{L_{ac}} \rightarrow K_{pi} = 2\omega_{ni}L_{ac} - R_{ac} \quad (30)$$

$$\frac{K_{ii}}{L_{ac}} = \omega_{ni}^2 \rightarrow K_{ii} = \omega_{ni}^2 L_{ac} \quad (31)$$

Note that the overall current at the DC-link, (I_i) in the VSC_i is $I_i = I_{ssi} + I_{hi}$, where I_{hi} is the harmonic content of the current due to the VSC_i switching & modulation and I_{ssi} is, in this approach, the linearized small-signal current at the DC link (I_{AFE} or I_{CPLi}), as depicted in Fig. 7.

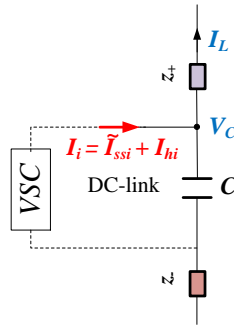


Fig. 7. Detail of the VSC DC-link.

E. The whole PEB-DCDS model

Once the outer grid, the inner grid and the VSC admittances are obtained, they can be mathematically ‘inter-connected’ to get the whole PEB-DCDS model (32). For that, it is strongly recommended the use of a computer based simulation tool to handle mathematically all the matrixes, for instance *Matlab*TM. Following with the example in Fig. 2, in (32) the matrix G_{DCDS} is the multivariable model, V_{DC}^* is the DC bus voltage set point, P_i^* are the loads’ active power set points and I_m and I_{sn} are the currents at the DC-link of the VSCs, see Fig. 8.

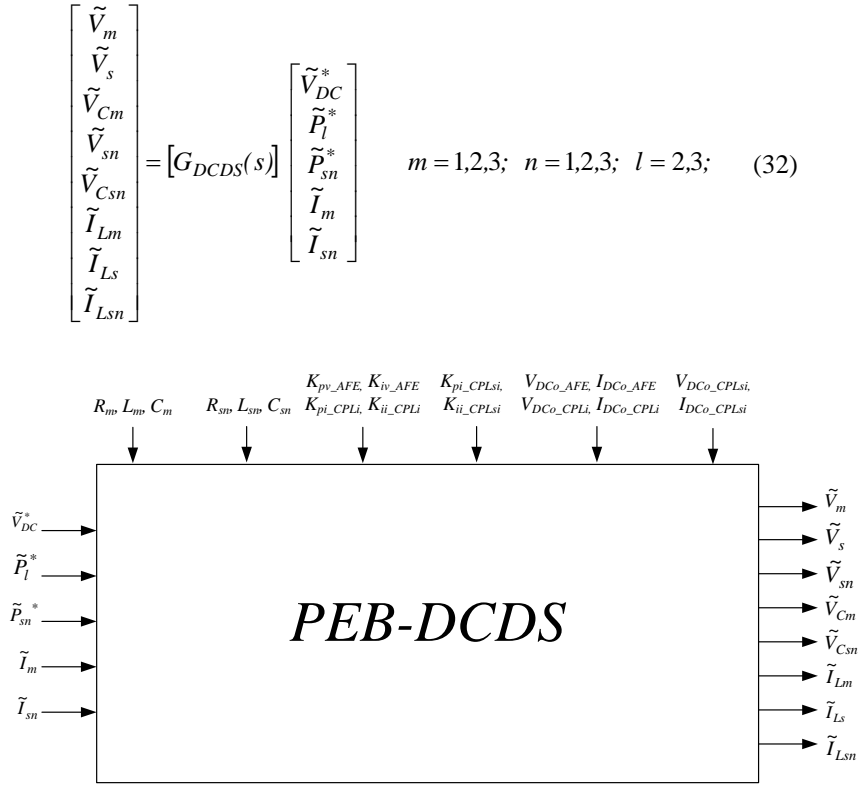


Fig. 8. Inputs and outputs of the whole PEB-DCDS mathematical model.

III. USEFULNESS OF THE MODEL

By the multivariable modeling approach previously described, different PEB-DCDS configurations can be evaluated and the variation of the DC currents and/or voltages from their equilibrium point can be analyzed in depth. The influence of different VSC control strategies can be evaluated too. Moreover, it is possible to study the dynamic behavior of the whole system in terms of stability and power quality in both, time and frequency domains. This section shows the usefulness of the model for such kind of analysis, by means of multivariable transfer functions analysis, Bode diagrams, pole maps or unit-step responses among others, in general, by means of the well-known linear systems control theory. For instance, a simple criterion for tuning the DC bus voltage regulator of the PEB-DCDS can be derived as one of the results. Additionally, the system resonances caused by the combination of the lines' parasitic impedances and the VSCs DC-link capacitors can be identified and then located. It results mandatory to identify these resonances because, depending on the frequency, magnitude and phase of these resonances, the whole system stability may deteriorate (low damped or even unstable PEB-DCDS). Moreover, the power quality of the PEB-DCDS (voltage and current ripples) can be affected too, especially when the main harmonics injected by the VSCs at their DC links (due to the switching operation and vector modulation technique) are located around the resonances of high magnitude.

A. Dynamic and Stability Analysis

Throughout this section, as an example for simplicity in the exposition, a possible design scenario of a PEB-DCDS with 3x branches is considered, in which 3x VSCs are connected (1x AFE-VSC and 2x CPL-VSCs) to a common DC bus, as depicted in Fig. 9. Note that all the analysis presented here, could be also applied to a PEB-DCDS with a different number of branches. The values of the electrical circuit parameters and the parameters used for the 3x VSCs are summarized in Table I and Table II respectively.

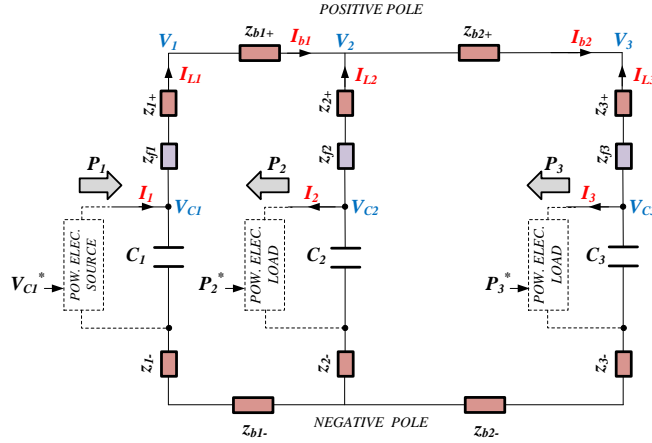


Fig. 9. 3x branches PEB-DCDS as a design example.

TABLE I. DC ELECTRICAL CIRCUIT PARAMETERS ESTIMATION, ACCORDING TO REAL DIMENSIONS AND MATERIAL OF THE BUS-DUCTS.

Parameter	Value
z_{1+}, z_{1-}	$R=300\mu\Omega, L=1.87\mu\text{H}$
z_{2+}, z_{2-}	$R=300\mu\Omega, L=1.87\mu\text{H}$
z_{3+}, z_{3-}	$R=300\mu\Omega, L=1.87\mu\text{H}$
z_{f1}, z_{f2}, z_{f3}	$R=0, L=0$
z_{b1+}, z_{b1-}	$R=108\mu\Omega, L=0.67\mu\text{H}$
z_{b2+}, z_{b2-}	$R=750\mu\Omega, L=4.71\mu\text{H}$
C_1, C_2, C_3	3.2mF

TABLE II. PARAMETERS OF THE VOLTAGE SOURCE CONVERTERS

Parameter	Values
LCL filter	$L_1=70\mu\text{H}, L_2=170\mu\text{H}, C=517.5\mu\text{F}$
f_{sw}	2500Hz
$V_{ac\ L-L}$	690V
Nominal power	500kW
V_{DCbus}	1100V
Modulation	PWM with 3 rd harmonic injection

Making use of the equations of the outer grid together with the VSC-admittance models, it is possible to obtain the transfer function matrixes of the whole closed-loop PEB-DCDS model for a general number of branches 'n'. For instance, in the case of a PEB-DCDS of 3x branches as depicted in Fig. 9, the matrix equations for the voltage in the DC-link of the VSC in branch 1, V_{C1} , and the DC current through the branch 1, I_{L1} , are defined by:

$$\tilde{V}_{C1} = \begin{bmatrix} G_{DCDS41}(s) & G_{DCDS42}(s) & G_{DCDS43}(s) \end{bmatrix} \cdot \begin{bmatrix} \tilde{V}_{C1}^* \\ \tilde{P}_2^* \\ \tilde{P}_3^* \end{bmatrix} \quad (33)$$

$$\tilde{I}_{L1} = \begin{bmatrix} G_{DCDS71}(s) & G_{DCDS72}(s) & G_{DCDS73}(s) \end{bmatrix} \cdot \begin{bmatrix} \tilde{V}_{C1}^* \\ \tilde{P}_2^* \\ \tilde{P}_3^* \end{bmatrix} \quad (34)$$

Being:

$$G_{DCDS41}(s) = \frac{b_0s^6 + b_1s^5 + b_2s^4 + b_3s^3 + b_4s^2 + b_5s + b_6}{a_0s^8 + a_1s^7 + a_2s^6 + a_3s^5 + a_4s^4 + a_5s^3 + a_6s^2 + a_7s + a_8} \quad (35)$$

$$G_{DCDS42}(s) = \frac{c_0s^4 + c_1s^3 + c_2s^2 + c_3s}{a_0s^8 + a_1s^7 + a_2s^6 + a_3s^5 + a_4s^4 + a_5s^3 + a_6s^2 + a_7s + a_8} \quad (36)$$

$$G_{DCDS43}(s) = \frac{d_0s^4 + d_1s^3 + d_2s^2 + d_3s}{a_0s^8 + a_1s^7 + a_2s^6 + a_3s^5 + a_4s^4 + a_5s^3 + a_6s^2 + a_7s + a_8} \quad (37)$$

$$G_{DCDS71}(s) = \frac{e_0s^5 + e_1s^4 + e_2s^3 + e_3s^2 + e_4s + e_5}{a_0s^8 + a_1s^7 + a_2s^6 + a_3s^5 + a_4s^4 + a_5s^3 + a_6s^2 + a_7s + a_8} \quad (38)$$

$$G_{DCDS72}(s) = \frac{f_0s^5 + f_1s^4 + f_2s^3 + f_3s^2 + f_4s + f_5}{a_0s^8 + a_1s^7 + a_2s^6 + a_3s^5 + a_4s^4 + a_5s^3 + a_6s^2 + a_7s + a_8} \quad (39)$$

$$G_{DCDS73}(s) = \frac{g_0s^5 + g_1s^4 + g_2s^3 + g_3s^2 + g_4s + g_5}{a_0s^8 + a_1s^7 + a_2s^6 + a_3s^5 + a_4s^4 + a_5s^3 + a_6s^2 + a_7s + a_8} \quad (40)$$

All the coefficients of the transfer functions ($a_0..a_8$, $b_0..b_6$, $c_0..c_3$, $d_0..d_3$, $e_0..e_5$, $f_0..f_5$ y $g_0..g_5$) can be obtained in both, symbolically by means of the ‘*Symbolic Math Toolbox*’ or numerically by using for instance the *Matlab*TM general environment (or other equivalent simulation tool). Note that all the terms in expressions (35)-(40), present the same denominator. It should be also noticed that the variables V_{C1} and I_{L1} depend on 3 different inputs (V_{C1}^* , P_2^* y P_3^*) given rise to a Multiple Input Multiple Output system.

By using the expressions (33), (34), the dynamic behavior of the whole original system can be analyzed. For instance, in Fig. 10, the poles map, the Bode diagram and the step response corresponding to the closed-loop transfer functions V_{C1}/V_{C1}^* and V_{C1}/P_3^* are depicted. Some information regarding the system dynamic behavior can be obtained. For instance, two resonances are noticed from the Bode Diagram, at 880Hz and 1340Hz respectively. From the Poles map, eight poles can be identified for both transfer functions: two complex conjugate poles (with dominant real part) related to the AFE-VSC voltage control loop dynamics, other two complex conjugate poles (with dominant real part) related to the VSC current control loop dynamics and two pairs of complex

conjugate poles related to the dynamic of the two system electrical resonances. It can be observed that the fastest two poles correspond to the current control loop dynamics which mainly depend on how the bandwidth of the VSCs' current loops have been designed (choice of K_{pi} and K_{ii}). On the other hand, the dominant poles or poles with slower dynamics, correspond to the DC voltage control loop dynamics which mainly depend on how the voltage loop control has been tuned (choice of K_{pv} and K_{iv}). Finally, in the middle of both, the two pairs of resonant poles are located in this example, which mainly depend on the impedances values of the equivalent electric circuit of the DC distribution system. The number of resonant pole pairs depends directly on the number of branches of the circuit. Consequently, there would be only one resonant pole pair in the case of 2x branches PEB-DCDS and three resonant pole pairs in the case of 4x branches PEB-DCDS. As can be seen from step responses and Bode diagrams of Fig. 10, for this particular 3x branches PEB-DCDS, the two resonances are significantly damped, and the entire dynamic response is mainly defined by the DC voltage control loop poles.

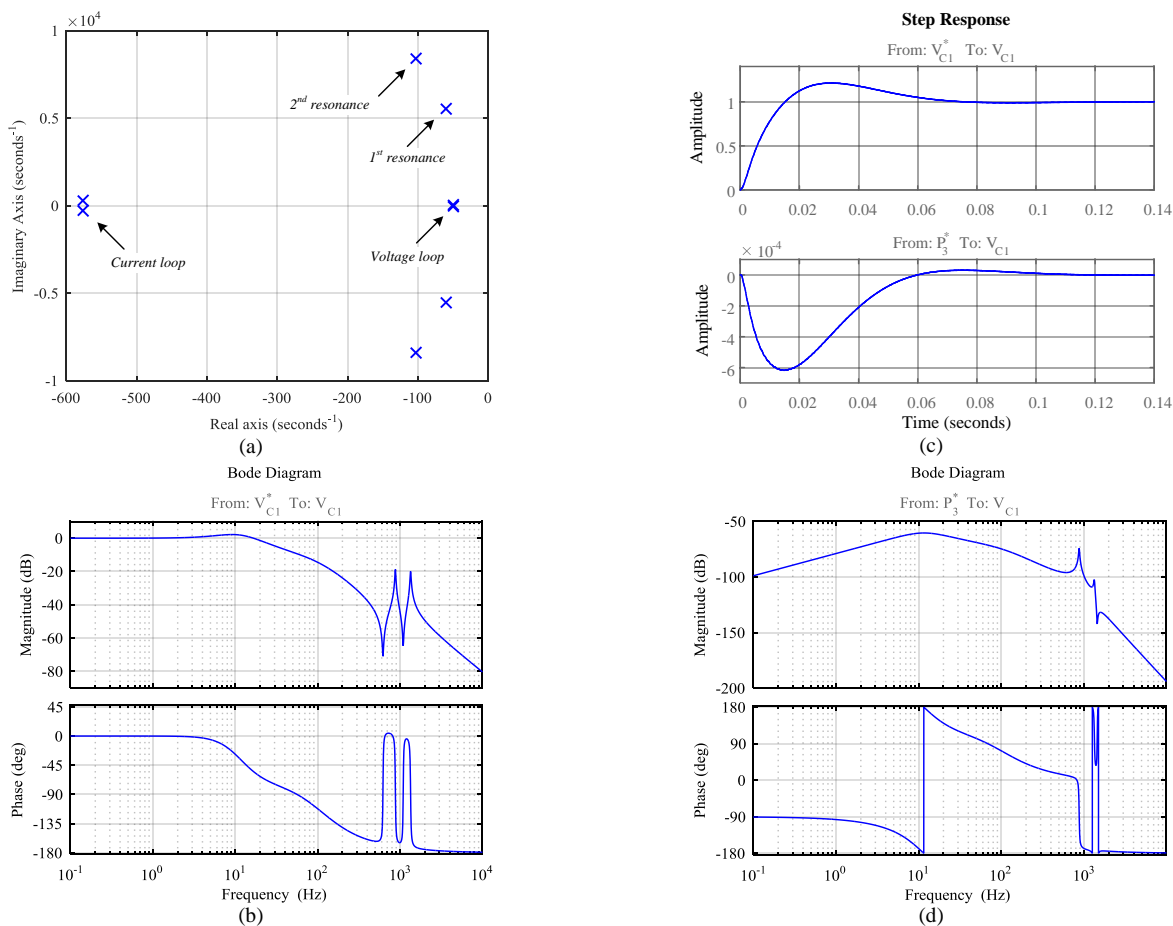


Fig. 10. Pole map (a), Bode diagram (b) of V_{C1}/V_{C1}^* transfer function. (c) unit-step response of V_{C1}/V_{C1}^* and V_{C1}/P_3^* transfer functions. (d) Bode diagram of V_{C1}/P_3^* transfer function. The equilibrium point for this analysis is $P_1=400\text{kW}$, $P_2=40\text{kW}$ and $P_3=360\text{kW}$.

The same analysis but for I_{L1}/V_{C1}^* and I_{L1}/P_3^* transfer functions is depicted in Fig. 11. In this case, the resonances are less damped than in the previous example (see the Bode Diagram), what means that at the Step Responses, the effect of the resonant poles is more significant. It is important to highlight that although the denominator (poles) is the same for all the different transfer

functions, the dynamic behavior can be different due to the location of the zeros, since the numerator of the transfer functions are different.

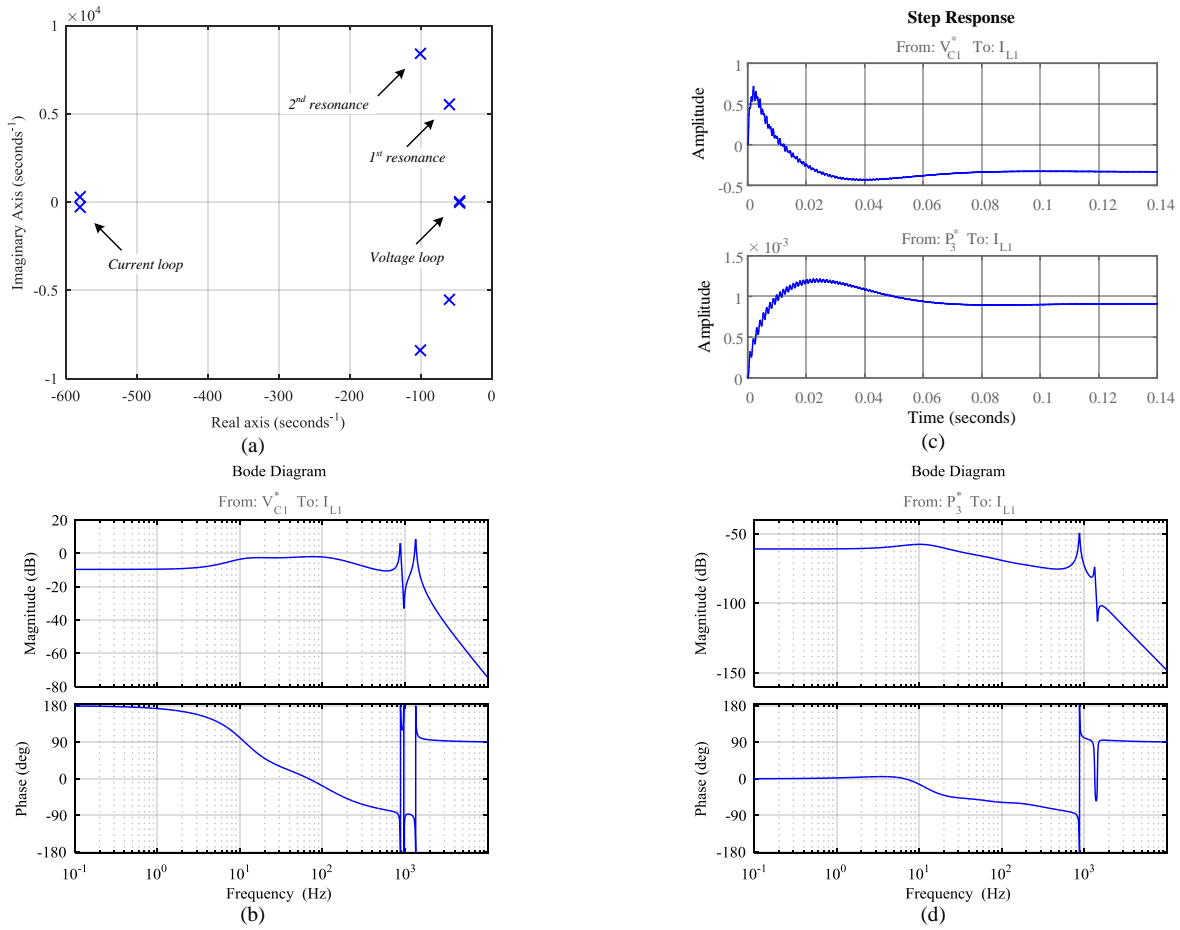


Fig. 11. Pole map (a), Bode diagram (b) of I_{L1}/V_{C1}^* transfer function. (c) Unit-step response of I_{L1}/V_{C1}^* and I_{L1}/P_3^* transfer functions. (d) Bode diagram of I_{L1}/P_3^* transfer function. The equilibrium point for this analysis is $P_1=400\text{kW}$, $P_2=40\text{kW}$ and $P_3=360\text{kW}$.

1) Tuning of DC voltage loop

A well-enough damped system with good stability margins for the representative operating points are not the unique/only requirement in terms of dynamic control. When the DC bus voltage experiences a high variation from its set point in order to reject the possible disturbances (for instance abrupt changes in the power demands), the system protections can actuate and stop the operation of the PEB-DCDS. In order to obtain a proper dynamic response of the DC bus voltage and avoid over-shoot from the limits imposed by the safety requirements, some dynamic response requirements must be considered. From these requirements, a mathematical criterion for tuning the DC bus voltage control loop is presented in this section. For the study, the symbolic equation for the transfer function V_{C1}/P_2^* (36) is used. That expression can be simplified by means of identifying the dominant terms of both the numerator and the denominator (41). The terms from expression (36): $a_0, a_1, a_2, a_3, a_4, a_5$ are numerically much smaller than a_5, a_6 and a_7 , and c_0, c_1, c_2 also are much smaller than c_3 . Therefore, they can be neglected in order to deduce the dominant dynamic behavior.

$$\frac{\tilde{V}_{C1}(s)}{\tilde{P}_2^*(s)} \cong \frac{c_3 s}{a_6 s^2 + a_7 s + a_8} \quad (41)$$

Then, from the symbolic analysis of the coefficients a_5 , a_6 , a_7 and c_3 , it is possible to observe their dependence on many parameters of the PEB-DCDS, resulting in quite long expressions that (due to lack of space) have not been included in the paper. Again, by finding out the dominant terms for these four coefficients, the simplified equivalent expression for V_{C1}/P_2^* transfer function is derived (42), (43):

$$\frac{\tilde{V}_{C1}(s)}{\tilde{P}_2^*(s)} = \frac{k_1 K_{ii} s}{\left(-n_{branches} CL_{ac} \omega_{ni}^2\right) s^2 + \left(k_1 K_{ii} K_{pv}\right) s + \left(k_1 K_{ii} K_{iv}\right)} \quad (42)$$

$$k_1 = \frac{1}{V_{C1o}} \quad (43)$$

This transfer function (42) depends on the grid parameters (L_{ac} , C and number of branches of the PEB-DCDS which in this case is 3), on the converter control parameters (ω_{ni} , K_{ii} , K_{pv} , K_{iv}) as well as on the DC bus voltage at the equilibrium/operating point, V_{C1o} . By repeating this procedure to the rest of the input/outputs V_{C1}/P_3^* , V_{C2}/P_2^* , V_{C2}/P_3^* , V_{C3}/P_2^* , V_{C3}/P_3^* , it is possible to see that these dominant terms are the same even considered a PEB-DCDS with different number of branches.

Therefore, by resembling the denominator of (42) to a standard second order system with damping factor $\zeta=1$, it is possible to define the parameters of the DC bus voltage PI controller, K_{pv} and K_{iv} , as (44)-(45):

$$2\omega_{nv} = \frac{k_1 K_{ii} K_{pv}}{-n_{branches} CL_{ac} \omega_{ni}^2} \rightarrow K_{pv} = \frac{2\omega_{nv} \left(-n_{branches} CL_{ac} \omega_{ni}^2\right)}{k_1 K_{ii}} \quad (44)$$

$$\omega_{nv}^2 = \frac{k_1 K_{ii} K_{iv}}{-n_{branches} CL_{ac} \omega_{ni}^2} \rightarrow K_{iv} = \frac{\omega_{nv}^2 \left(-n_{branches} CL_{ac} \omega_{ni}^2\right)}{k_1 K_{ii}} \quad (45)$$

Accordingly, the natural frequency ω_{nv} can be defined as in (46), the overshoot M_p in volts for certain predefined maximum step of power P_{step} for P_2^* as in (47) and a peak time as in (48).

$$\omega_{nv} = \frac{k_1 K_{ii}}{n_{branches} CL_{ac} \omega_{ni}^2} \frac{0.368}{M_p} P_{step} \frac{1}{V_{C1o}} \quad (46)$$

$$M_p = \frac{0.368}{\omega_{nv}} \quad (47)$$

$$t_p = \frac{1}{\omega_{nv}} \quad (48)$$

Consequently, by means of the simple expressions (44)-(48), it is possible to keep the DC bus voltage of the PEB-DCDS, under a safe operation region as depicted in Fig. 12, thus fulfilling the dynamic control requirements defined for the DC bus voltage. As depicted in Fig. 12, going below the minimum voltage limit can cause loss of control of the system, due to a lack of bus voltage, whereas the maximum limit is to avoid damage of the system due to over-voltage. Both situations can derive into unstable operation of the PEB-DCDS and this information is not noticeable at classic stability analysis based on pole analysis for instance. Therefore, it must be highlighted that the tuning of the DC bus voltage loop should be also defined in order to reject sudden and abrupt changes on the power demands thus ensuring not losing control. When the maximum power step demand happens, ' P_{step} ', the voltage at the DC-link of the converter will not cross the threshold of the safe operation region. At the same time, the dynamic time response also is defined (t_p). Hence, ensuring that the voltage limits are not exceeded for all the operation modes, is essential for an optimal design of a vessel with PEB-DCDS, where sudden power demands are common when the propellers get into/out of the water, or when strong waves or wind gusts occurs for instance.

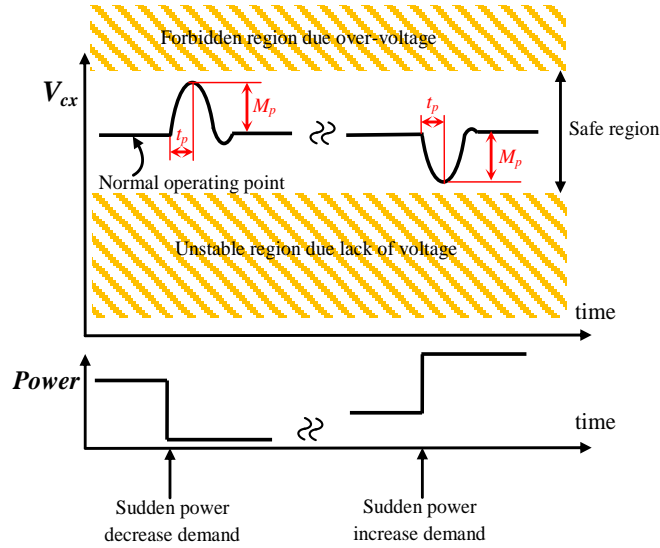


Fig. 12. DC bus voltage limitations under a sudden power demand.

The validation of this method for tuning the DC bus voltage controller is shown in Fig. 13. For that, a power step of 100kW is applied to P_2^* for two different maximum over-voltage values: $M_p = 50V$ ($t_p = 14.35ms$) and $M_p = 75V$ ($t_p = 21.5ms$).

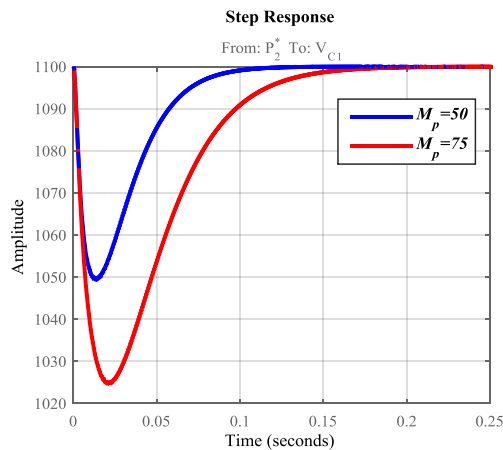


Fig. 13. DC bus voltage response after a power step of 100kW in P_2^* .

2) Effect of system parameters

When analyzing the stability and the dynamic behavior of any system, it is mandatory to know the location of the poles of the system and study their displacement in function of the values of the different design variables/parameters of the PEB-DCDS. By means of the mathematical model presented in this paper, the influence of some design parameters into the whole system dynamic behavior can be then analyzed. For that, a variation in the value of such parameters has been considered. The parameters under variation are: the impedance of the bus-bars and cables (resistance and inductance), the DC link capacitance of the VSCs, the DC bus voltage control parameters of the AFE-VSC, the current control parameters of the VSCs, and the vessel operating point (the power demands and the power load sharing). The range of variation for each parameter is detailed in Table III. The transfer function corresponding to the voltage of the AFE-VSC DC link and the active power set-point in the branch 3, i.e. V_{C1}/P_3^* , has been considered as an example for this study. Some of the results are shown in Fig. 14 (through the poles map, Bode diagrams and step responses), in which the evolution of the poles of the system and the frequency response can be analyzed in function of the parameters' variation. A summary of the effect of these parameters variations is shown in Table IV. According to the possible unstable scenarios it can be concluded that mainly the resonant poles could cross to the real plane especially in the cases of too small parasitic resistance, high parasitic inductances, as well as in certain combinations of load power demands.

TABLE III. VARIATION RANGE OF PARAMETERS

Parameter	Variation range	
	Min.	Max.
R	$R(x, bx, fx)_{nom}/10$	$R(x, bx, fx)_{nom} \times 5$
L	$L(x, bx, fx)_{nom}/4$	$L(x, bx, fx)_{nom} \times 10$
C_{bus}	$C_{bus}/2$	$C_{bus} \times 7$
M_p	20	70
$K_{pi} \ \& \ K_{ii}$	$(K_{pi} \ \& \ K_{ii})_{nom}/10$	$(K_{pi} \ \& \ K_{ii})_{nom} \times 10$
$O.P. \ AFE$	400kW	3MW

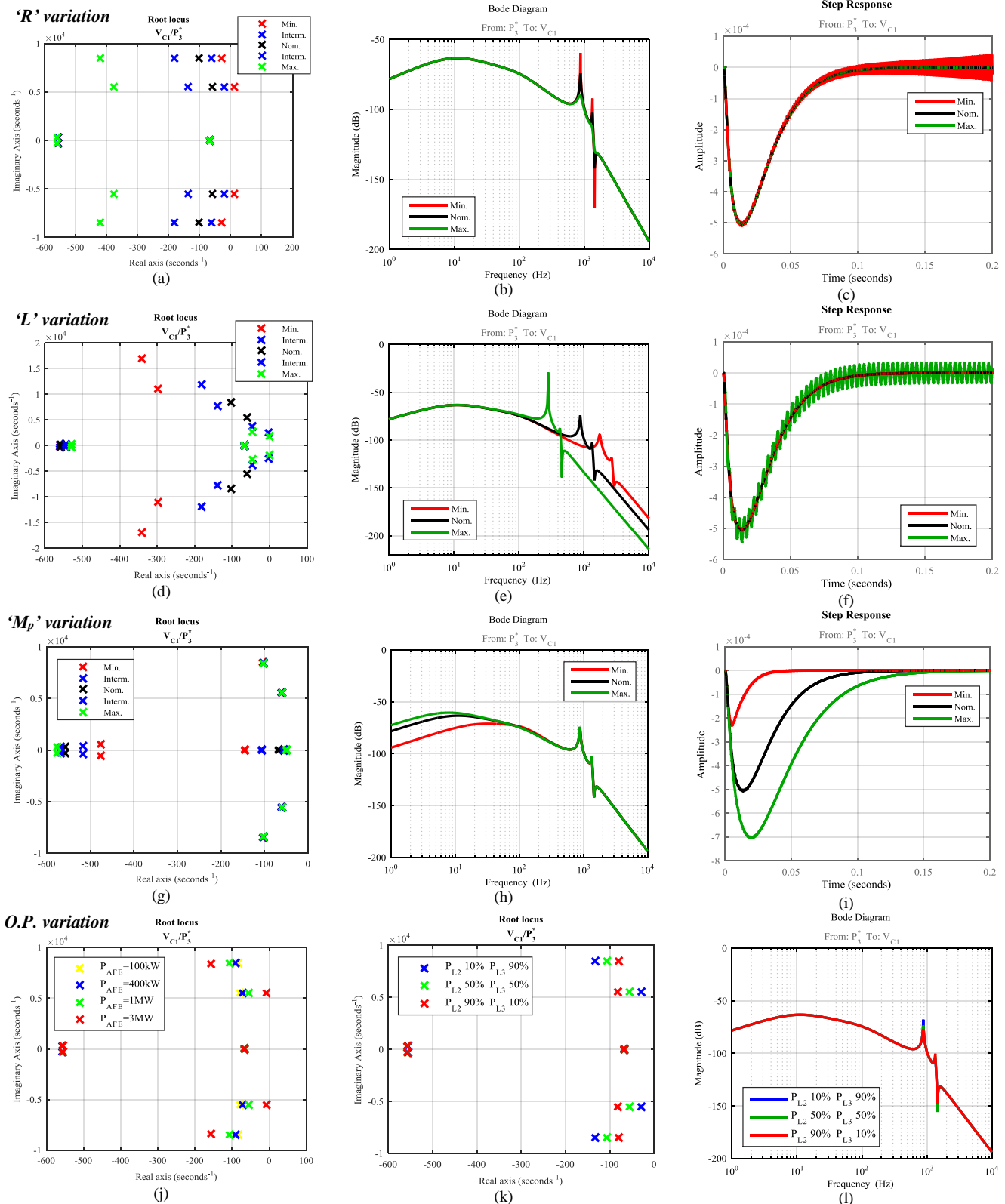


Fig. 14. Dynamic analysis by the Poles map, Bode diagram and unit-step response for system parameters variation. (a)(b)(c) Resistance variation. (d)(e)(f) Inductance variation. (g)(h)(i) Maximum over-voltage ' M_p ' variation. (j) Operating point variation with equal power sharing between P_2^* and P_3^* . (k)(l) Power sharing variation with equal operating point ($P_{AFE}^*=1MW$).

TABLE IV. MAIN CONCLUSIONS OF THE PARAMETERS VARIATIONS

	Poles related to the current loop	Poles related to the voltage loop	Poles related to the resonances of the DC grid
'R' Variation	Does not affect.	Does not affect.	Modifies the real part of the poles. Modifies the amplitude of the resonances and the oscillations in the transient response.
'L' Variation	Does not affect.	Does not affect.	Modifies the real and imaginary part of the poles. Modifies the amplitude and the frequency of the resonances and the oscillations in the transient response.
'C_{bus}' Variation	Modifies slightly the real part of the poles and the dynamics of the loop.	Modifies the real part of the poles and the dynamics of the loop.	Modifies the real and imaginary part of the poles. Modifies the amplitude and the frequency of the resonances and the oscillations in the transient response.
M_p Variation (K_{pv} & K_{iv} variation)	Modifies slightly the real and imaginary part of the poles and the dynamics of the loop.	Modifies the real and imaginary part of the poles and the dynamics of the loop.	Does not affect.
K_{pi} & K_i Variation	Modifies the real part of the poles and the dynamics of the loop.	Does not affect.	Does not affect.
O.P. Variation	Does not affect.	Does not affect.	Modifies the real part of the poles. Modifies the amplitude of the resonances and the oscillations in the transient response.

B. Power Quality Analysis

The power quality analysis is recommendable from the early design stages in order to fulfill the requirements established by the designers and by the Class Societies [28], [29]. Moreover, high signal ripples on the DC currents and voltages in the PEB-DCDS steady-states can degrade the system performance in terms of energy losses, heating, and cost due to the oversizing of components. High signal ripples are generally due to the harmonic content of the currents at the DC-link of the VSCs produced by the switching and modulation of the converters. The AC side voltage and currents harmonics are transferred to the DC side of the distribution system by means of the converter. On the other hand, the harmonics depend on the modulation used, on the VSCs switching frequency as well as on the vessel operating point.

In this paper, some few general considerations to analyze the power quality of the PEB-DCDS voltages and currents are provided. They are mainly based on the analysis of the Bode diagrams corresponding to the transfer functions V_{Cx}/I_x and I_{Lx}/I_x together with the spectrum analysis of the harmonic content of modulation used at each converter. A detailed analysis related to the influence of the modulation strategy in a three-phase VSC on the harmonic content of the current injected at the DC link can be found in [30]. In order to carry out the power quality analysis, the harmonic content produced by the modulation must be considered into the PEB-DCDS model through its addition to the small-signal input variables \tilde{I}_m or \tilde{I}_{sn} . The system is highly coupled so the harmonic content of all the VSCs affect the DC grid currents and voltages. Consequently, the transfer functions to be considered in a PEB-DCDS with 3x branches when focusing on V_{C1} and I_{L1} are shown in (49) and (50), where all the transfer

functions ($G_{DCDS44}(s)$, $G_{DCDS45}(s)$, $G_{DCDS46}(s)$, $G_{DCDS74}(s)$, $G_{DCDS75}(s)$, $G_{DCDS76}(s)$) can be numerically obtained, for instance, using the *Matlab*TM environment

$$\tilde{V}_{C1} = [G_{DCDS44}(s) \quad G_{DCDS45}(s) \quad G_{DCDS46}(s)] \cdot \begin{bmatrix} \tilde{I}_1 \\ \tilde{I}_2 \\ \tilde{I}_3 \end{bmatrix} \quad (49)$$

$$\tilde{I}_{L1} = [G_{DCDS74}(s) \quad G_{DCDS75}(s) \quad G_{DCDS76}(s)] \cdot \begin{bmatrix} \tilde{I}_1 \\ \tilde{I}_2 \\ \tilde{I}_3 \end{bmatrix} \quad (50)$$

As an example, the Bode diagram of the transfer functions I_{L1}/I_1 , I_{L1}/I_2 , I_{L1}/I_3 , V_{C1}/I_1 , V_{C1}/I_2 and V_{C1}/I_3 is shown in Fig. 15, where the attenuation or amplification of the harmonics injected by the VSCs at their DC-links can be easily observed. Therefore and applying the principle of superposition it could be easy to anticipate the harmonic content (ripple) of the current and voltage at the branch 1, I_{L1} and V_{C1} .

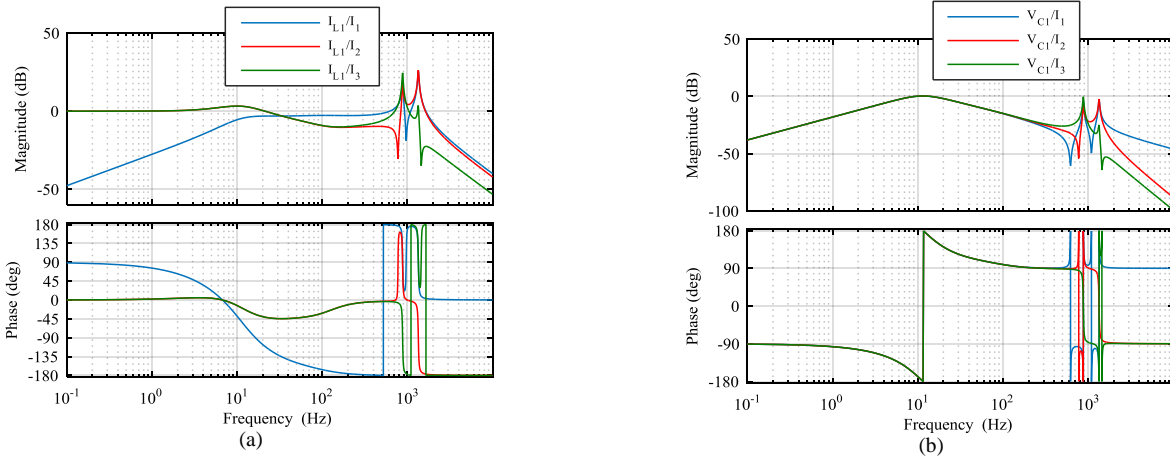


Fig. 15. Bode diagram of the transfer functions I_{L1}/I_1 , I_{L1}/I_2 , I_{L1}/I_3 , V_{C1}/I_1 , V_{C1}/I_2 and V_{C1}/I_3 is depicted.

Another way to analyze the power quality could be by executing some simulations in the time-domain. For that, the exact harmonic content (magnitude and phase/phase-shift) of the modulation technique is superimposed onto the small-signal current of the converter at the DC-link, see Fig. 7. The time domain simulation including the spectrum analysis of V_{C1} and I_{L1} of the 3x branches PEB-DCDS from Fig. 9 under a modulation of type ‘Pulse Width Modulation’ at a switching frequency of 2.5kHz are shown in Fig. 16.

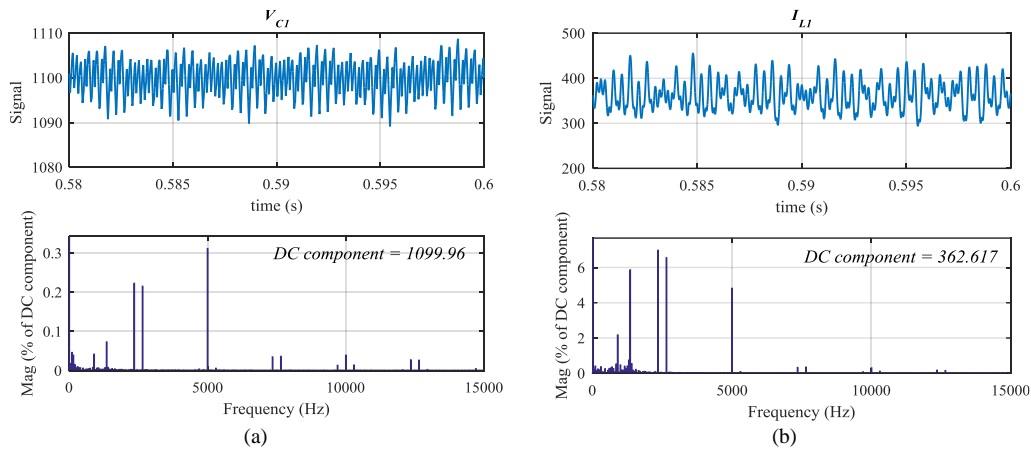


Fig. 16. Spectrum analysis of the voltage V_{CI} and the current I_{LI} of the 3x branches PEB-DCDS when applying the 'Pulse Width Modulation' technique with a switching frequency of 2.5kHz.

Some active damping control strategies can be proposed in order to mitigate the effects of the resonances of low damped PEB-DCDS. The active damping control strategy from [11] can be added at every controlled VSC on the PEB-DCDS (load and sources). It could be only and automatically activated when the resonances are excited, therefore not consuming current or power at normal steady-state operation. Comparing to the alternative of passive filters, there is not extra investment or space required, since the active damping loop can be incorporated into the VSC control software architecture. Note that knowing where the resonances of the PEB-DCDS are located, helps to a correct choice of the switching frequency of the converters and vice-versa, since both the system resonances and switching frequency, should be sufficiently away one from each other aiming to avoid not only power harmonic problems, but stability problems as well.

In conclusion, not only the small-signal stability analysis but also the influence of the current harmonics injected by the VSCs can be deeply studied and evaluated by the mathematical model proposed in this paper.

IV. SIMULATION AND EXPERIMENTAL RESULTS

The validation of the proposed model has been carried out by using the *Matlab*TM & *Simulink*TM environment and also over a real test bench (experimental set-up). On the one hand, a complete 4x branches PEB-DCDS (including the VSCs with their vector control, PWM modulation, and 3-phase 2-level IGBTs based converters IngedriveTM LV400 (Ingeteam Power Technology [31]) has been modeled using the *SimPowerSystems*TM toolbox. Although a 3x branches PEB-DCDS has been used in the previous section for an easier exposition, the validation of the model has been carried out with a more complex 4x branches PEB-DCDS. The VSCs have been modelled in a realistic manner including their most important nonlinearities due to the switching, modulation, discretization, control delays, measurement delays, etc. The simulation with this more accuracy model has, however, a high computational cost compared to the one required for the mathematical model proposed in this work.

and the current of the branch 1 (I_{L1}), the Bode diagram of Fig. 19 can be constructed. The Bode diagram obtained by using the mathematical model and the one obtained experimentally in the test bench are shown in Fig. 19 for comparative purpose.

A system with 4x branches has three resonances but, due to the configuration and design of the test bench, only two resonances are noticeable in the Bode diagram (a third very damped resonance is located at 1280Hz). It can be noticed how the resonances are a little more attenuated in reality and slightly moved to the right. According to the different analysis presented before, this information means that in the real test bench there is a little bit more resistance and less inductance than the theoretically estimated. This mismatch is due to the fact that all the specific connections and junctions inside the power stacks and along the DC bus have not been considered. However, this experiment demonstrates that the theoretical method [23] is a very useful and accurate enough tool to model the parasitic inductances of the PEB-DCDS, obtaining a good and accurate estimation of the frequency bands where the system resonances are located.

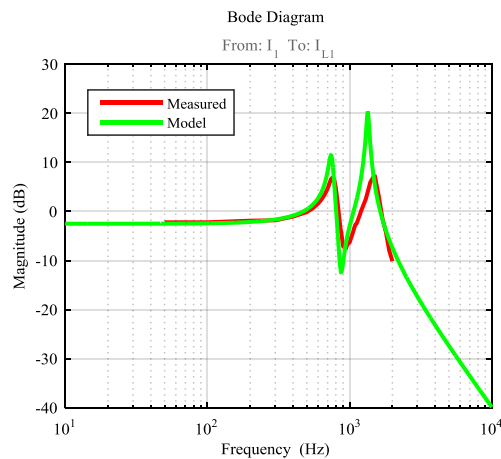


Fig. 19. Measured and theoretically calculated Bode diagram of I_{L1}/I_1 transfer function.

The second issue to be experimentally proven is the dynamic response of the currents and voltages of the PEB-DCDS. For that, different tests in different test bench configurations have been carried out. First, in a 4x branch configuration, with all the converters operating (1x AFE & 3x CPL), some voltage steps of $\pm 50V$ are applied to the DC bus voltage set point, V_{CI}^* . The voltage at the DC-link of VSC₁, V_{CI} , and the branch currents I_{L1} and I_{L2} obtained by the analytical small-signal model (the one proposed in this work), the *Matlab*TM & *Simulink*TM & *SimPowerSystems*TM non-linear high-signal model, and finally the experimentally measured ones from the test bench are superimposed in Fig. 20.

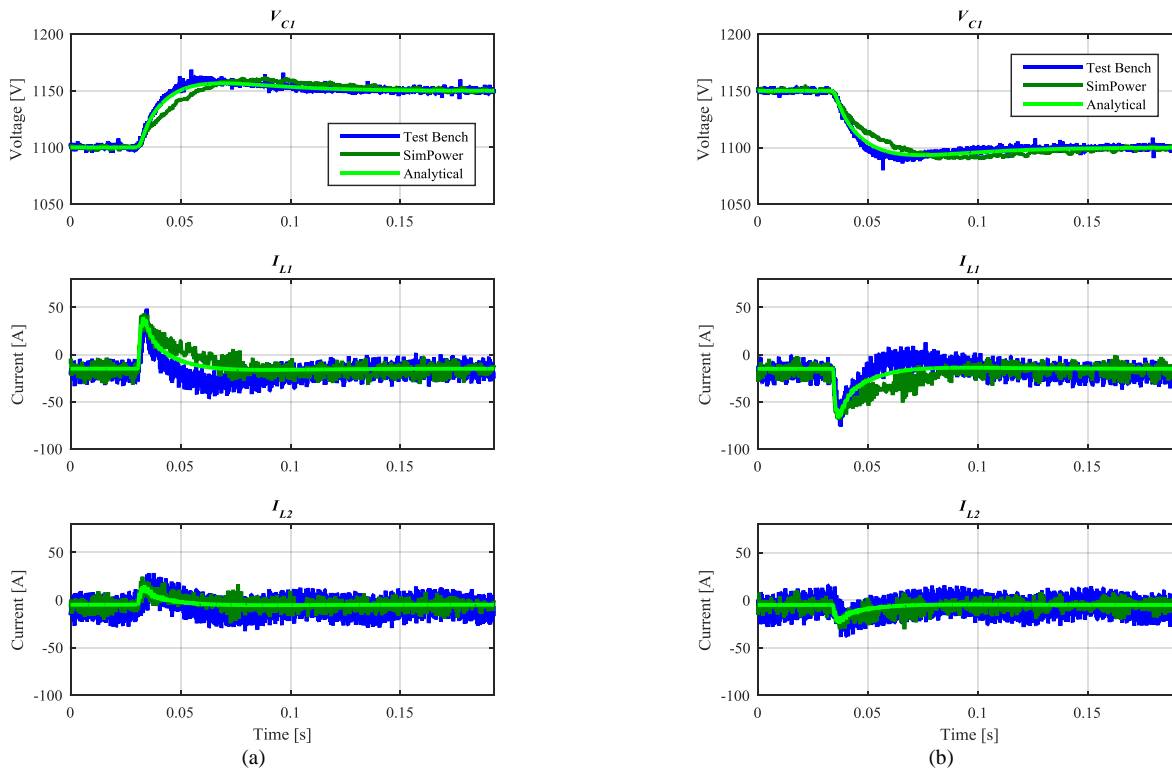


Fig. 20. Voltage steps in V_{C1}^* in a PEB-DCDS with 4x branches. (a) V_{C1} , I_{L1} and I_{L2} for a positive voltage step (+50V). (b) V_{C1} , I_{L1} and I_{L2} for a negative voltage step (-50V).

It can be observed that the theoretical models and the experimental results match quite well, and then the dynamic response of the test bench, tuned and controlled as described in section III, behaves as predicted by the mathematical model.

The behavior of the system under sudden power variations has been also validated. For that purpose, the experimental test bench was configured to operate with 2x branches connected to the DC grid, i.e. one AFE-VSC and one CPL-VSC. Power variations of $\pm 100\text{kW}$ were programmed at CPL_1 , P_2^* , with a slew rate of 5MW/s (sufficiently close to an idealistic step). Two set of experiments were performed; the first one with the voltage controller tuned at ' M_p '=50V and the second one at ' M_p '=75V. In Fig. 21, it is seen how, the proposed analytical small-signal model, the *Matlab*TM & *Simulink*TM & *SimPowerSystems*TM non-linear high-signal model and the experimental results on the test bench match reasonably well. Note that since the power variation is not a pure step, the DC bus voltage does not reach the 50V and 75V peaks.

Hence, all these results validate the effectiveness of the proposed average small-signal multivariable model in the small-signal transient response, in the resonance location and at steady-state. Therefore, it is corroborated that the multivariable modeling approach could be a useful tool for design and analysis of PEB-DCDS.

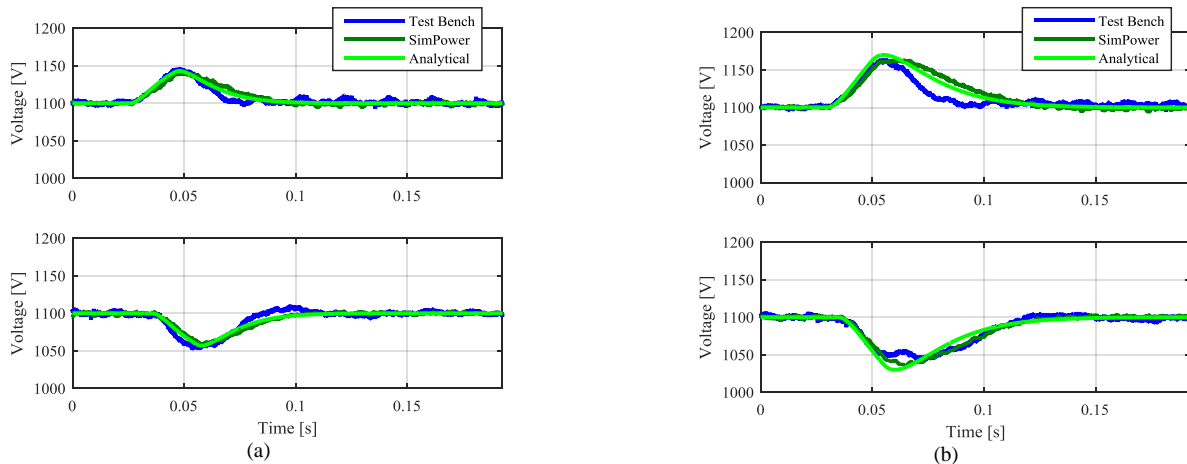


Fig. 21. V_{C1} after a step in P_2^* in a PEB-DCDS with 2x branches. (a) Step of $\pm 100\text{kW}$ and $M_p=50$. (b) Step of $\pm 100\text{kW}$ and $M_p=75$.

V. CONCLUSIONS

A multivariable and high order mathematical model for the design of PEB-DCDS in electrically propelled vessels is proposed in this work. In the proposed modeling approach, scenarios in which one or more sub/inner PEB-DCDS are connected to a main/outer PEB-DCDS are considered. Through this model, such analyses as the stability, the dynamic control behavior or the power quality can be addressed from the early design stages at low computational cost. Added to this, this model can support the design and tuning of the PEB-DCDS active control strategies in an analytical and theoretical way. The model is demonstrated to work by means of a complete non-linear simulation environment and also in a real test bench of 2MW, showing its effectiveness.

When a PEB-DCDS optimal design is pursued, a low computational cost model is needed as fitness function to evaluate the objectives of the problem for different sets of design variables. On the searching of the best design solution, an iterative process could be launched and be conducted by the designers or by an optimization algorithm. The model proposed in this work can be used for the design optimization of the PEB-DCDS from the early design stages due to its low computational cost.

As future works, this modeling approach philosophy could easily integrate progressive extensions such as: inclusion of DC-DC converters for energy storage and renewable generation, inclusion of control techniques for autonomous operation of AFE rectifiers (droop control strategies or others), consideration of different nature converters as for instance Medium Voltage converters, or short circuit analysis, among others.

VI. REFERENCES

- [1] A. Opdahl, "Fuel Savings Obtained by Replacing Traditional AC-distribution Systems onboard Vessels with DC-distribution Systems," NTNU - Trondheim. Norwegian University of Science and Technology, 2013.
- [2] J. F. Hansen, J. O. Lindtjorn, and K. Vanska, "Onboard DC Grid for enhanced DP operation in ships," in *MTS Dynamic Positioning Conference*, 2011.
- [3] A. Emadi, A. Khaligh, C. H. Rivetta, and G. A. Williamson, "Constant power loads and negative impedance instability in automotive systems: Definition, modeling, stability, and control of power electronic converters and motor drives," *IEEE Trans. Veh. Technol.*, vol. 55, no. 4, pp. 1112–1125, 2006.
- [4] M. Karbalaye Zadeh, R. Gavagsaz ghoachani, S. Pierfederici, B. Nahid-Mobarakeh, and M. Molinas, "Stability Analysis and Dynamic Performance

- Evaluation of A Power Electronics-Based DC Distribution System With Active Stabilizer,” *IEEE J. Emerg. Sel. Top. Power Electron.*, vol. 6777, no. c, pp. 1–1, 2015.
- [5] A. Riccobono and E. Santi, “A novel Passivity-Based Stability Criterion (PBSC) for switching converter DC distribution systems,” *Conf. Proc. - IEEE Appl. Power Electron. Conf. Expo. - APEC*, pp. 2560–2567, 2012.
- [6] S. D. Sudhoff, S. F. Glover, S. H. Zak, S. D. Pekarek, E. J. Zivi, D. E. Delisle, and D. Clayton, “Stability analysis methodologies for DC power distribution systems,” in *Proceedings of the 13th International Ship Control Systems Symposium*, 2003.
- [7] A. Riccobono and E. Santi, “Comprehensive Review of Stability Criteria for DC Power Distribution Systems,” *IEEE Trans. Ind. Appl.*, vol. 50, no. 5, pp. 3525–3535, Sep. 2014.
- [8] M. Karbalaye Zadeh, R. Gavagsaz-Ghoachani, J.-P. Martin, S. Pierfederici, B. Nahid-Mobarakeh, and M. Molinas, “Discrete-time modelling, stability analysis, and active stabilization of dc distribution systems with constant power loads,” *Conf. Proc. - IEEE Appl. Power Electron. Conf. Expo. - APEC*, vol. 2015–May, no. May, pp. 323–329, 2015.
- [9] J. Siegers, S. Arrua, and E. Santi, “Stabilizing Controller Design for Multi-Bus MVDC Distribution Systems Using a Passivity Based Stability Criterion and Positive Feed-Forward Control,” *IEEE J. Emerg. Sel. Top. Power Electron.*, pp. 1–1, 2016.
- [10] M. Hamzeh, M. Ghafouri, H. Karimi, K. Sheshyekani, and J. M. Guerrero, “Power Oscillations Damping in DC Microgrids,” *IEEE Trans. Energy Convers.*, vol. 31, no. 3, pp. 970–980, Sep. 2016.
- [11] A. Alacano, G. Abad, and J. J. Valera-García, “Active Damping Control Strategy to Avoid Resonance Issues in Diesel-Electric Vessels with DC Distribution Systems,” in *17th IEEE Workshop on Control and Modeling for Power Electronics, COMPEL, 2016*, 2016.
- [12] T. Dragicevic, X. Lu, J. Vasquez, and J. Guerrero, “DC Microgrids – Part I: A Review of Control Strategies and Stabilization Techniques,” *Power Electron. IEEE Trans.*, vol. PP, no. 99, p. 1, 2015.
- [13] T. Dragicevic, X. Lu, J. C. Vasquez, and J. M. Guerrero, “DC Microgrids - Part II: A Review of Power Architectures, Applications and Standardization Issues,” *IEEE Trans. Power Electron.*, vol. 31, no. 5, pp. 3528–3549, May 2016.
- [14] E. Unamuno and J. A. Barrena, “Primary control operation modes in islanded hybrid ac/dc microgrids,” *Proc. - EUROCON 2015*, pp. 1–6, 2015.
- [15] E. Unamuno and J. A. Barrena, “Hybrid ac/dc microgrids - Part II: Review and classification of control strategies,” *Renew. Sustain. Energy Rev.*, vol. 52, pp. 1123–1134, 2015.
- [16] L. Yang, Y. Chen, A. Luo, W. Wu, K. Huai, X. Zhou, L. Zhou, Q. Xu, and J. M. Guerrero, “Second Ripple Current Suppression by Two Band-Pass Filters and Current Sharing Method for Energy Storage Converters in DC Microgrid,” *IEEE J. Emerg. Sel. Top. Power Electron.*, vol. 6777, no. c, pp. 1–1, 2016.
- [17] E. A. A. Coelho, D. Wu, J. M. Guerrero, J. C. Vasquez, T. Dragičević, Č. Stefanović, and P. Popovski, “Small-Signal Analysis of the Microgrid Secondary Control Considering a Communication Time Delay,” *IEEE Trans. Ind. Electron.*, vol. 63, no. 10, pp. 6257–6269, 2016.
- [18] J. J. Valera-García and I. Atutxa-Lekue, “Sistemas Integrados de Potencia en Buques Offshore: Control, tendencias y retos,” *Rev. Iberoam. Automática e Informática Ind. RIAI*, vol. 13, no. 1, pp. 3–14, 2016.
- [19] L. Qi, A. Antoniazzi, L. Raciti, and D. Leoni, “Design of Solid State Circuit Breaker Based Protection for DC Shipboard Power Systems,” *IEEE J. Emerg. Sel. Top. Power Electron.*, vol. 6777, no. c, pp. 1–1, 2016.
- [20] R. Mo and H. Li, “Hybrid Energy Storage System with Active Filter Function for Shipboard MVDC System Applications Based on Isolated Modular Multilevel DC/DC Converter (IM2DC),” *IEEE J. Emerg. Sel. Top. Power Electron.*, vol. 6777, no. c, pp. 1–1, 2016.
- [21] R. Soman, M. Steuer, T. Toshon, M. O. Faruque, and R. M. Cuzner, “Size and Weight Computation of MVDC Power Equipment in Architectures Developed Using the Smart Ship Systems Design Environment,” *IEEE J. Emerg. Sel. Top. Power Electron.*, vol. 6777, no. c, pp. 1–1, 2016.
- [22] S. Caniggia and F. Maradei, *Signal Integrity and Radiated Emission of High-Speed Digital Systems*. Wiley, 2008.
- [23] C. Hoer and C. Love, “Exact Inductance Equations for Rectangular Conductors With Applications to More Complicated Geometries,” *J. Res. Natl. Bur. Stand. - C. Eng. Instrum.*, vol. 69C, No.2, 1965.
- [24] A. Ametani, T. Ohno, and N. Nagaoka, *Cable System Transients*. Singapore: John Wiley & Sons, Singapore Pte. Ltd, 2015.
- [25] G. Abad, *Power electronics and electric drives for traction applications*. John Wiley & Sons, 2016.
- [26] R. Teodorescu and M. Liserre, *Grid converters for photovoltaic and wind power systems*, vol. 29. John Wiley & Sons, 2011.
- [27] R. W. Erickson and D. Marsimovic, “Fundamentals of Power Electronics, Kluwer Academic Publishers,” *Norwell, MA*, 2001.
- [28] S. Nadarajan, A. K. Gupta, and S. K. Panda, “Review of smart grid requirements and design standards for future Naval vessels,” in *2016 IEEE International Conference on Sustainable Energy Technologies (ICSET)*, 2016, pp. 338–343.
- [29] Y. Khersonsky, “New IEEE Power Electronics Standards for Ships.”
- [30] M. Bierhoff and F. W. Fuchs, “DC link harmonics of three phase voltage source converters influenced by the pulse width modulation strategy-an analysis,” *31st Annu. Conf. IEEE Ind. Electron. Soc. 2005. IECON 2005.*, pp. 491–496, 2005.
- [31] “Ingeteam.” [Online]. Available: www.ingetteam.com.